⌘ *Author's Choice*

THE JOURNAL OF BIOLOGICAL CHEMISTRY VOL. 286, NO. 40, pp. 35051–35060, October 7, 2011

Structural Basis for the Allosteric Interference of Myosin Function by Reactive Thiol Region Mutations G680A and G680V*

Received for publication, May 31, 2011, and in revised form, August 1, 2011 Published, JBC Papers in Press, August 13, 2011, DOI 10.1074/jbc.M111.265298

Matthias Preller[‡], Stefanie Bauer[‡], Nancy Adamek[§], Setsuko Fujita-Becker[¶], Roman Fedorov[‖], Michael A. Geeves[§], and Dietmar J. Manstein[‡¶‖1]

From the [‡]Institut für Biophysikalische Chemie and the [‖]Forschungseinrichtung für Strukturanalyse, Medizinische Hochschule Hannover, Carl-Neuberg-Strasse 1, 30625 Hannover, Germany, the [§]Department of Biosciences, University of Kent, Canterbury, Kent CT2 7NJ, United Kingdom, and the [¶]Max-Planck-Institut für Medizinische Forschung, Jahnstrasse 29, 69120 Heidelberg, Germany

Background: Cold-sensitive mutations in the reactive thiol region of myosin interfere with motor function.
Results: Structural and functional data indicate that the mutations induce the preferential population of a state that resembles the ADP-bound state.
Conclusion: Gly-680 mutations lead to uncoupling of the reactive thiol region from the surrounding structural elements.
Significance: Our results explain how moderate increases in temperature suppress the mutant defects.

The cold-sensitive single-residue mutation of glycine 680 in the reactive thiol region of *Dictyostelium discoideum* myosin-2 or the corresponding conserved glycine in other myosin isoforms has been reported to interfere with motor function. Here we present the x-ray structures of myosin motor domain mutants G680A in the absence and presence of nucleotide as well as the apo structure of mutant G680V. Our results show that the Gly-680 mutations lead to uncoupling of the reactive thiol region from the surrounding structural elements. Structural and functional data indicate that the mutations induce the preferential population of a state that resembles the ADP-bound state. Moreover, the Gly-680 mutants display greatly reduced dynamic properties, which appear to be related to the recovery of myosin motor function at elevated temperatures.

The reactive thiol region is a structurally well conserved region in the C-terminal part of the lower 50 (L50)[2]-kDa domain of the myosin motor domain that corresponds to a broken α-helix. The two helix fragments are referred to as SH1 (residues 681–689) and SH2 helices (residues 669–678), named for two reactive cysteine residues found in skeletal muscle myosins. The sulfhydryl groups of the two cysteine residues in this region can be chemically cross-linked by a variety of reagents, bridging distances of 2–18 Å (1–4). Myosin with SH1 and SH2 cross-linked within a distance of 3 Å is predicted to hold the nucleotide "trapped" in the active site with no measurable ATPase activity (4). Chemical modifications of SH1 and SH2 result in dramatic alteration of myosin ATPase activity and actin binding affinity (5, 6). In *Dictyostelium discoideum* myosin-2, one of these thiol positions (SH1) is occupied by a threonine residue (Thr-688) (7). It has been suggested that changes in the nucleotide state of the active site lead to conformational changes in the reactive thiol region (2, 8). In fact, the reactive thiol region together with the adjacent structural elements, the relay helix and the central seven-stranded β-sheet, also referred to as the transducer, are involved in the transmission of energetic information from the active site to the mechanical amplifier region, the converter and the lever arm, during the chemomechanical myosin cycle. Thus, the reactive thiol region participates in coupling the state of the active site to the converter/lever arm position and plays a key role in force generation by myosin motors.

The reactive thiol region of *Dd* myosin-2 contains three conserved glycine residues, namely Gly-680, Gly-684, and Gly-691. Mutations of Gly-680 are of particular interest as it is in the immediate vicinity of the fulcrum point for lever arm movement. Mutation of Gly-680 to an alanine or valine residue leads to large changes in binding affinity toward different nucleotides (9–12). Both mutants, G680A and G680V, show low ATPase activity and poor motility (13, 14). The rate of ATP and ADP binding to G680A is reduced 16–30-fold. However, ADP binds 10-times tighter to the protein due to a 200-fold decrease in the ADP off rate (11). In contrast, binding of ATP and ADP to acto-G680A is faster than binding to wild-type constructs. Additionally, the second order rate constant for ADP binding is increased ~2.5-fold compared with that for ATP binding in the presence of actin. Actin is still capable of accelerating both the rates of ADP binding and ADP release up to 62-fold, but it does not reduce the affinity of G680A for ADP, as the ratio of K_{AD}/K_D is close to 1 (11). In contrast, a ratio of 14 was deter-

* This work was supported in part by Wellcome Trust Grant 085309 (to M. A. G.) and grants from Deutsche Forschungsgemeinschaft Ma 1081/16-1 and the Cluster of Excellence "Rebirth" (to D. J. M.).
⌘ *Author's Choice*—Final version full access.
The atomic coordinates and structure factors (codes 2Y0R, 2Y8I, and 2Y9E) have been deposited in the Protein Data Bank, Research Collaboratory for Structural Bioinformatics, Rutgers University, New Brunswick, NJ (http://www.rcsb.org/).
[1] To whom correspondence should be addressed. Tel.: 49-511-5323700; Fax: 49-511-5325966; E-mail: manstein.dietmar@mh-hannover.de.
[2] The abbreviations used are: L50, lower 50; U50, upper 50; SH, Src homology; MD, molecular dynamics; M765-1R, *Dd* myosin-2 motor domain construct comprising residues 1–765, fused to a C-terminal α-actinin repeat; acto×G680A, G680A mutant in complex with filamentious actin.

mined for the wild-type motor domain construct (11). Elevated temperatures were shown to compensate the mutant defects and rescue myosin activity (12, 15).

Despite the large amount of biochemical data for the Gly-680 mutants and their impact on myosin motor function, the mechanism underlying the interference of myosin activity by mutations of residue Gly-680 remains still elusive. Here we present the x-ray crystallographic analysis of *Dd* myosin-2 motor domain mutants G680A and G680V. Structural analysis of the mutant motor domains in combination with transient kinetic experiments and molecular dynamics simulations provides information about the communication between the nucleotide binding pocket and the converter domain and provides an explanation for the rescue of myosin motor function at increased temperatures.

EXPERIMENTAL PROCEDURES

The equilibrium dissociation constant for ADP binding to *Dd* myosin-2 motor domain in the presence and absence of actin is defined as K_{AD} ($=k_{-AD}/k_{+AD}$) and K_D ($=k_{-D}/k_{+D}$), respectively, where the rate constant of ADP association is k_{+i}, and the rate constant of dissociation is k_{-i}.

Protein Preparation and Mutagenesis—His_8-tagged motor domain Gly-680 mutant constructs of *Dd* myosin-2 comprising amino acids 1–765 fused to a C-terminal α-actinin repeat were generated as described elsewhere (11) and purified using Ni^{2+}-chelate affinity chromatography (16).

Rabbit skeletal muscle actin was prepared as described by Lehrer and Kerwar (17) and labeled with pyrene iodoacetamide as described previously (18).

Stopped Flow Experiments and Fluorescence Titration—Stopped flow experiments were performed for transient kinetic measurements at 20 °C with a Hi-Tech SF61 stopped flow spectrophotometer equipped with 100-watt Xe/mercury lamps and a monochromator. Pyrene fluorescence on rabbit actin was excited at 365 nm and detected after passing through a KV 389 nm cutoff filter. Intrinsic tryptophan fluorescence on myosin, excited at 295 nm, was monitored through a WG 320 nm cutoff filter (Schott, Mainz). Data were stored and analyzed using software provided by Hi-Tech Scientific (Salisbury, UK). Unless stated otherwise, the experimental buffer was 20 mM MOPS (pH 7.0), 5 mM $MgCl_2$, and 100 mM KCl.

Crystallization, Data Collection, and Refinement—Crystals of the purified *Dd* myosin-2 motor domain Gly-680 mutants were obtained at 4 °C by vapor diffusion using the sitting drop geometry. The nucleotide-bound G680A complex crystals were grown in the presence of 2 mM ADP, 2 mM sodium *meta*-vanadate, and 2 mM $MgCl_2$. One microliter of protein and reservoir solutions was mixed. In the case of the crystallization of the apo form of the G680A mutant, the reservoir solution contained 100 mM MES buffer (pH 6.5) and 25% (w/v) PEG 8000, whereas for nucleotide-bound G680A, the reservoir solution contained 13% (w/v) PEG 6000 and 4% (v/v) glycerol. Conditions for the growth of G680V mutant crystals were 100 mM HEPES (pH 7.5) and 20% PEG 10,000 as reservoir solutions. 50-μm pencil-shaped crystals grew after several weeks of incubation. Before flash-cooling, crystals were rinsed in a cryo-protection solution consisting of 100 mM MES (pH 6.5), 25% (w/v) PEG 8000, 150 mM NaCl, and 10% (v/v) ethylene glycol for apoG680A crystals, 100 mM HEPES (pH 7.5) and 20% PEG 10,000, 150 mM NaCl, and 10% (v/v) ethylene glycol for apoG680V crystals, and 14% (w/v) PEG 6,000, 150 mM NaCl, 25% (v/v) ethylene glycol, and 5% (v/v) glycerol for G680A-ADP crystals.

Diffraction data were collected at the European Synchrotron Radiation Facility microfocus beamlines ID13 (G680A and

TABLE 1
ADP dissociation rate constants and activation energies of *D. discoideum* myosin constructs

Construct	k_{-D} (20 °C)	$\Delta H^{\ddagger}$	Arrhenius factor
	s^{-1}	$kJ{\cdot}mol^{-1}$	
−Actin			
M765-1R	7.4	94.2	42
G680A	0.06	54.9	20
+Actin			
M765-1R	215[a]		
G680A	1.0	41.3	17

[a] This value was taken from Ref. 11.

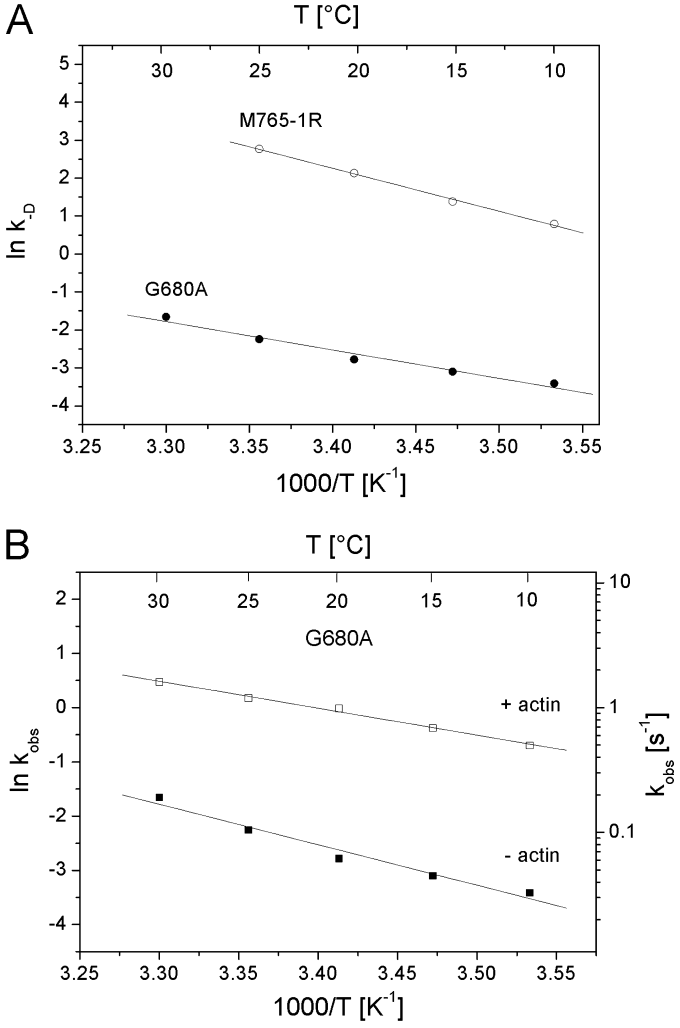

FIGURE 1. **Arrhenius plot.** *A*, shown is temperature dependence of the ADP off-rate (k_{-D}) of M765-1R and G680A in the absence of actin. The datasets were fitted to a linear equation giving the activation energy $\Delta H^{\ddagger}$ of 94.16 $kJ{\cdot}mol^{-1}$ for M765-1R and 54.9 $kJ{\cdot}mol^{-1}$ for G680A. *B*, shown is temperature dependence of the ADP off-rate of G680A in the absence (k_{-D}) and presence (k_{-AD}) of actin. The data sets were fitted to a linear equation giving the activation energy $\Delta H^{\ddagger}$ of 54.9 ± 7.5 $kJ{\cdot}mol^{-1}$ without actin and 41.3 ± 1.7 $kJ{\cdot}mol^{-1}$ in the presence of actin.

Diffraction data were collected at the European Synchrotron Radiation Facility microfocus beamlines ID13 (G680A and

TABLE 2
ADP affinities and thermodynamic parameters of *D. discoideum* myosin constructs

Construct −actin	$K_{D\ (20\ °C)}$	$\Delta G^{o}_{20\ °C}$	ΔH^{o}	ΔS^{o}	$-T\Delta S^{o}_{20\ °C}$
	μM	$kJ{\cdot}mol^{-1}$	$kJ{\cdot}mol^{-1}$	$J{\cdot}K^{-1}{\cdot}mol^{-1}$	$kJ{\cdot}K^{-1}{\cdot}mol^{-1}$
M765-1R	7.5	28.7	65.7	126.3	−36.9
G680A	2	32	84.0	175.4	−51.6
Construct + actin	$K_{AD\ (20\ °C)}$	$\Delta G^{o}_{20\ °C}$	ΔH^{o}	ΔS^{o}	$-T\Delta S^{o}_{20\ °C}$
	μM	$kJ{\cdot}mol^{-1}$	$kJ{\cdot}mol^{-1}$	$J{\cdot}K^{-1}{\cdot}mol^{-1}$	$kJ{\cdot}K^{-1}{\cdot}mol^{-1}$
M765-1R	243	20.3	11.2	−34.9	10.2
G680A	0.5	35.3	30.3	−10.0	2.9

G680V apo form) and ID23-2 (G680A-ADP complex) using ADSC Quantum 4 CCD detector and reduced with the XDS program package (19). Molecular replacement was carried out with Amore (20) using PDB 1MMD coordinates as the starting model, and model refinement was performed using Refmac5 (21) and Phenix 1.6 (22). A random 5% of the data was excluded for cross-validation. Model building and validation were carried out using COOT (23).

Molecular Dynamics Simulations and Principal Component Analysis—All molecular dynamics simulations were carried out with the Gromacs 4.0 software package (24) and the OPLS (Optimized Potentials for Liquid Simulations) all-atom force field (25). The simulations were performed in explicit solvent using the TIP4P water model (26). Starting coordinates were taken from the G680A and G680V x-ray structures (PDB IDs 2Y0R and 2Y9E). For the simulations of the wild type, coordinates of the *Dd* myosin-2 motor domain in the rigor state were used (PDB ID 2AKA). MD simulations were performed in a *NpT* ensemble at 300 K and 1 bar using Berendsen temperature coupling and Parrinello-Rahman pressure coupling. Long-range electrostatics were treated with particle-mesh Ewald (27) with a grid spacing of 0.12 nm and an interpolation order of 4. Short-range van der Waals and coulomb forces were treated with 14 and 10 Å cutoffs, respectively. A 2 fs time step was used during the production runs, and all bond lengths were constrained with the LINCS algorithm (28). After initial energy minimization with the steepest descent algorithm to a force of 1000 $kJ{\cdot}mol^{-1}{\cdot}nm^{-1}$, the coordinates were optimized with the conjugate gradient algorithm to a final force of <10 $kJ{\cdot}mol^{-1}{\cdot}nm^{-1}$. The solvent molecules were equilibrated for 100 ps. Subsequently, equilibration of the entire system was carried out for ~4 ns, during which the root mean square deviation of the backbone atoms reached a plateau. Production runs were performed for 100 ns. *In silico* mutation experiments were based on the wild-type coordinates, in which glycine 680 was replaced either by alanine or valine. Parameters were used as described above. Production runs lasted for 100 ns. Computation and diagonalization of the covariance matrix of the molecular dynamics (MD) trajectories to obtain the eigenvectors and eigenvalues for principal component analysis were performed with Gromacs.

RESULTS

Temperature Dependence of the Rate of ADP Dissociation (k_{-D} and k_{-AD})—In the absence of actin the rates of ADP dissociation from the myosin motor domain for the wild-type (M765-1R) and G680A mutant were determined by monitoring the time dependence of the change in Trp fluorescence upon displacement of ADP from the myosin complex by the addition of ATP. The results are in good agreement with previously published data (11), where a single exponential transient was observed under saturating conditions (>40 μM ADP) and $k_{obs} = k_{-D}$ (rate constant of ADP release from myosin construct). The ADP release rate constant for the G680A mutant in the absence of actin was dramatically slower (by a factor of 100) than for the wild-type with k_{-D} (20 °C) = 0.063 s^{-1}, compared with 7.4 s^{-1} for wild-type (Table 1). The maximum dissociation rate constant increased from 1.6 s^{-1} at 10 °C to 15.2 s^{-1} at 25 °C for the wild type and from 0.038 s^{-1} at 10 °C to 0.18 s^{-1} at 30 °C for the G680A mutant. An Arrhenius plot for the temperature dependence of the ADP dissociation rate in the absence of actin is shown in Fig. 1*A*. Fitting the data to a linear equation gives activation energies of $\Delta H^{\ddagger} = 94.2 \pm 3.1$ $kJ{\cdot}mol^{-1}$ for the wild type and $\Delta H^{\ddagger} = 54.9 \pm 7.5$ $kJ{\cdot}mol^{-1}$ for G680A; thus, a 2-fold difference in activation enthalpy for G680A over wild type. In the presence of actin the ADP release constants, k_{-AD}, were monitored by the single exponential change observed in pyrene fluorescence upon displacement of ADP from the actomyosin complex by ATP (under saturating conditions). In the presence of actin, the ADP release rate constant from acto-G680A was accelerated 10–15-fold, k_{-AD} (20 °C) = 0.99 s^{-1}, whereas the wild type showed 30-fold acceleration (k_{-AD} (20 °C) = ~215 s^{-1} (11)). The temperature dependence of k_{-AD} of G680A showed similar behavior compared with the absence of actin with an activation energy reduced by about 14 $kJ{\cdot}mol^{-1}$ to $\Delta H^{\ddagger} = 41.3 \pm 1.7$ $kJ{\cdot}mol^{-1}$ (Fig. 1*B*).

Temperature Dependence of ADP Affinity (K_D and K_{AD})—The ADP affinities (K_D) of wild type and mutant constructs in the absence of actin at different temperatures were measured by monitoring the Trp fluorescence change upon ATP-induced ADP displacement from the myosin motor domain at different ADP concentrations. The transients were fitted to a double exponential equation, and the amplitudes of the fast phase were plotted against the ADP concentration to obtain ADP affinities of K_D (20 °C) = 6.6 μM for the wild-type and K_D (20 °C) = 1.3 μM for G680A at 20 °C (Fig. 2, *A* and *B*). Thermodynamic parameters were obtained by fitting the K_D values at different temperatures in the Van't Hoff plot to a linear equation (Fig. 2*C*). Calculating the free Gibbs energy according to $\Delta G^{o} = -k_B T{\cdot}\ln K_D$ from the 20 °C data, there is only a small difference in the free energy between wild type and mutant myosin $\Delta\Delta G^{o} \approx 4$ $kJ{\cdot}mol^{-1}$ (~10%). Nevertheless, a 25% difference in enthalpy ΔH^{o} was observed, compensated by large positive entropy change ΔS^{o} of similar size (~25% difference) (Table 2).

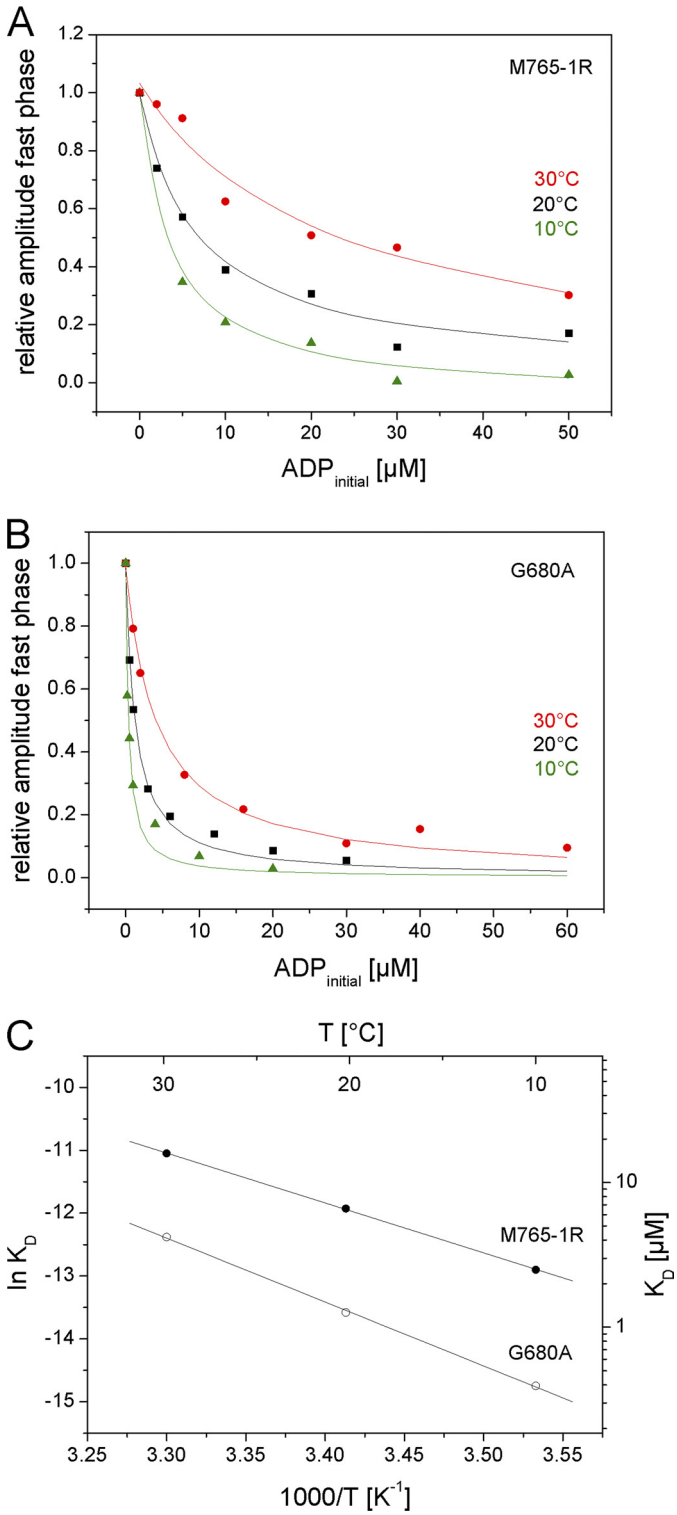

FIGURE 2. **Temperature dependence of K_D for wild-type (M765-1R) and G680A.** *A*, ADP affinity K_D of wild type in the absence of actin at different temperatures is shown. 0.5 μM M765-1R preincubated with various concentrations of ADP was mixed in the stopped flow with 1 mM ATP at different temperatures, and the change in Trp fluorescence was monitored over time. The transients were fitted to a double-exponential equation, and the amplitudes of the fast phase were normalized (relative $A_{fast} = A_{fast}/A_{total}$). Relative amplitudes of the fast phase were plotted against the ADP and fitted to a hyperbola to obtain the K_D of M765-1R (2.5 μM at 10 °C, 6.6 μM at 20 °C, and 15.9 μM at 30 °C). *B*, ADP affinity K_D of G680A in the absence of actin at different temperatures. 0.5 μM G680A with various concentrations of ADP is mixed with 400 μM ATP at different temperatures monitoring the change in Trp fluorescence. The transients were fitted to a double-exponential equation, and the amplitudes of the fast phase were normalized (relative $A_{fast} = A_{fast}/A_{total}$). The relative amplitudes of the fast phase were plotted against the ADP. The data sets were fitted to a hyperbola to obtain the ADP affinity K_D for each temperature (0.39 μM at 10 °C, 1.26 μM at 20 °C, and 4.2 μM at 30 °C). *C*, a Van't Hoff plot is shown. Temperature dependence of the K_D of M765-1R and G680A in the absence of actin is shown. The data sets were fitted to a linear equation. The slope of M765-1R was −7.9 ± 0.1 K and of G680A −10.1 ± 0.3 was K. $\Delta H°$(M765-1R) = 65.7 kJ/mol, $\Delta S°$ = 126.3 J/Kmol, $\Delta H°$ (G680A) = 84.8 kJ/mol, and $\Delta S°$ = 175.4 J/Kmol.

The affinity of ADP for pyrene-labeled actomyosin (K_{AD}) was determined from the inhibition of ATP-induced dissociation of the complex in the presence of ADP. In the case of acto-wild type the ADP was preincubated with the ATP (ATP/ADP competition approach). Single exponential transients were observed, and the k_{obs} is plotted as a function of ADP and fitted to a hyperbola ($k_{obs} = (K_1[ATP])/(1 + ([ADP]/K_{AD})$ to obtain the ADP affinities in the presence of actin (Table 2). Due to the much tighter ADP affinity expected with G680A, the ADP inhibition approach was used for the mutant. Here the ADP was preincubated with the acto·G680A, and on mixing with ATP double exponential transients were observed (where the fast phase represents ATP binding to acto·G680A, whereas the slow phase represents ADP release from acto·G680A). Plots of the fast phase amplitudes as a function of ADP were fitted to a hyperbola to obtain the K_{AD} values. No significant change in K_{AD} was observed for the wild type at different temperatures, but the G680A mutant showed an ~100-fold tighter affinity for ADP than the wild-type myosin, with a slight temperature dependence (Fig. 3, *A* and *B*). The enthalpy $\Delta H°$ and entropy $\Delta S°$ changes of the mutant were about 3-fold higher than those of the wild type (Fig. 3*C*). Upon the addition of actin, a decrease of more than 8 kJ·mol^{-1} of the free energy $\Delta G°$ was observed for the wild-type myosin, but an increase by 3 kJ·mol^{-1} was measured for G680A. Therefore, the affinity of wild-type myosin for ADP decreases rapidly upon binding of actin, whereas it is much less affected in the G680A mutant (Table 2).

Structural Consequence of Gly-680 Mutation—X-ray crystal structures were obtained for G680A (PDB ID 2Y0R) and G680V (PDB ID 2Y9E) mutants in the absence of nucleotide as well as G680A in complex with ADP (PDB ID 2Y8I). The G680A and G680V apo structures were refined up to resolutions of 2.85 and 3.4 Å, respectively (Table 3). Both apo state motor domain structures are very similar to each other but differ greatly from the previously published structure of the nucleotide-free *D. discoideum* wild-type motor domain (PDB ID 2AKA (29)) as well as from other apo-state wild-type myosins of class 2 (PDB IDs 3I5G, 3I5H, 2EC6, 3I5H, 3I5G, and 2OS8 (30)) and class 5 (PDB IDs 1OE9 (31) and 1W8J (32)). Typical for post-powerstroke structures, the mutant structure relay helices are straight, and the converters are in the down position. Critical differences are a widening of the 50-kDa cleft in the mutant structures, with the width of the cleft being similar to those of wild-type structures in the presence of ATP analogues. Further rearrangements are observed for the γ-phosphate sensors of the active site. The P-loop projects deeper into the nucleotide binding pocket. The salt bridge between Arg-238 (Switch-1) and Glu-459 (Switch-2) is broken. Switch-2 is moved away from switch-1 (Fig. 4*A*). The high similarity of the new mutant struc-

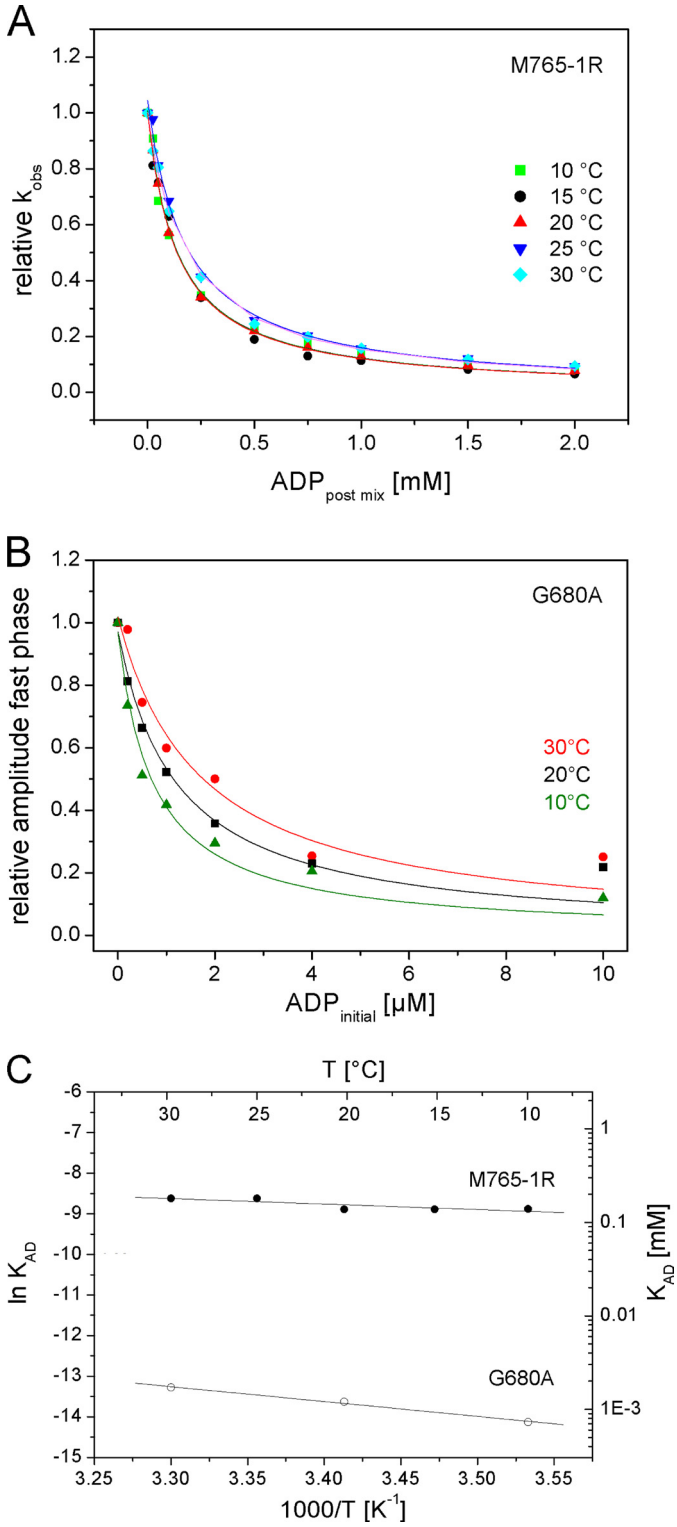

FIGURE 3. **Temperature dependence of K_{AD} of wild type and G680A.** *A*, ADP affinity K_{AD} of M765-1R in the presence of actin at different temperatures (ATP/ADP competition approach) is shown. 0.5 μM pyrene-actin-M765-1R was mixed with 1 mM ATP with various concentrations of ADP present, and the single-exponential change in Pyr fluorescence was monitored over time at different temperatures. The k_{obs} data were normalized (relative $k_{obs} = k_{obs}/k_{obs}$ at zero ADP), plotted as a function of ADP, and fitted to a hyperbola to obtain the ADP affinity K_{AD} of M765-1R at each temperature (0.138 mM at 10 °C, 0.137 mM at 15 °C, 0.137 mM at 20 °C, and 0.18 mM at 25 and 30 °C). *B*, ADP affinity K_{AD} of G680A in the presence of actin at different temperatures (ADP inhibition approach) is shown. 0.5 μM pyrene-Act-G680A preincubated with various concentrations of ADP was mixed with 200 μM ATP at different temperatures, and the biphasic change in pyrene fluorescence was monitored over time. The amplitudes of the fast phase were normalized (relative $A_{fast} = A_{fast}/A_{total}$), plotted as a function of ADP, and fitted to a hyperbola to obtain the K_{AD} of G680A at each temperature (0.73 μM at 10 °C, 1.2 μM at 20, and 1.7 μM at 30 °C). *C*, a Van't Hoff plot is shown. Temperature dependence of the K_{AD} of M765-1R and G680A in the presence of actin is shown. The data sets were fitted to a linear equation, giving the slopes as -1.35 ± 0.48 K for M765-1R and -3.6 ± 0.3 K for G680A. $\Delta H°$(M765-1R) = 11.2 ± 4.0 kJ/mol, $\Delta S°$(M765-1R) = -34.9 ± 14.1 J/mol, $\Delta H°$(G680A) = 30.3 ± 2.5 kJ/Kmol, and $\Delta S°$(G680A) = -10.0 ± 8.3 J/Kmol.

tures to the x-ray structures of *D. discoideum* myosin-2 in complex with ADP (PDB IDs 1MMA, 1JWY, 1JX2, and 1G8X) confirms the Gly-680 mutant apo structures to adopt a state that resembles the ADP-bound state. Nevertheless, comparing the mutant structures with the published ADP-bound structures, there are striking differences in the interaction pattern of the reactive thiol region and the relay helix as well as the transducer.

The ADP-bound state is defined by an open 50-kDa cleft, Switch-2 in the open position with the critical salt bridge between Arg-238 and Glu-459 unformed, the transducer untwisted, an unkinked relay helix, and the converter and lever arm in the down position. Available x-ray structures of the *D. discoideum* myosin motor domain in the ADP-bound state (33–36) show an extensive hydrogen bonding pattern of the reactive thiol region to the relay helix and the transducer that clusters around the SH1/SH2-linker loop, where Gly-680 is located (Fig. 5). Interactions between the reactive thiol region and the third strand (β3) of the transducer include hydrogen bonds between Gln-675$^{SH1/SH2}$ and the main chain of Ile-657$^{\beta3}$ as well as direct hydrogen bonds between Asn-679$^{SH1/SH2}$ and Arg-654$^{\beta3}$ and a water network that couples the reactive thiol region to the transducer through the residues Arg-654$^{\beta3}$, Cys-655$^{\beta3}$, Gln-675$^{SH1/SH2}$, and Asn-679$^{SH1/SH2}$. Furthermore, hydrogen bonds are formed between Gln-479^{relayhelix} and Arg-654$^{\beta3}$, and a water-mediated interaction occurs between Gln-479^{relayhelix}, Asn-483^{relayhelix}, and Glu-683$^{SH1/SH2}$ as well as a water-mediated hydrogen bond between the main chain carbonyl group of Leu-478^{relayhelix} and Arg-654$^{\beta3}$. The latter interactions facilitate the communication between the long relay helix of the lower 50-kDa domain to the reactive thiol region and the transducer. In contrast, most of these interactions between the reactive thiol region and the relay helix or central β-sheet were found to be broken in the Gly-680 mutant structures. The introduction of an aliphatic side chain, alanine or valine, at position 680 leads to a displacement of the reactive thiol region of about 2–3 Å away from the relay helix, with a root mean square deviation of about 2.2–2.7 Å.

Furthermore, the G680A mutant structure in complex with nucleotide was solved up to a resolution of 3.13 Å. The nucleotide analog ADP-VO_3 was used for the crystal setups to trap the myosin motor domain in the pre-power stroke state. However, despite the use of 2 mM ADP and 2 mM sodium *meta*-vanadate during crystallization, no electron density has been found for the γ-phosphate mimicking VO_3 anion in the nucleotide binding pocket (Fig. 4*B*). Moreover, the G680A-ADP complex structure shows a typical ADP-bound state of the myosin motor domain instead of a pre-power stroke state that would be expected in the presence of ADP-VO_3. The P-loop, Switch-1,

TABLE 3
Summary of data collection and refinement statistics

	G680A (apo)	G680A·ADP	G680V (apo)
Data collection			
Space group	$P22_12_1$	$P22_12_1$	$P22_12_1$
Wavelength (Å)	0.9175	0.9175	0.9175
Cell dimensions			
a, *b*, *c* (Å)	54.6, 106.0, 178.9	55.5, 106.5, 184.0	55.0, 105.8, 180.5
α, β, γ (°)	90, 90, 90	90, 90, 90	90, 90, 90
R_{sym} (%)[a]	18.3 (46.5)	16.8 (46.5)	14.0 (52.5)
$I/\sigma I$	8.53 (2.61)	9.23 (2.37)	7.34 (2.44)
Completeness (%)	98.31 (85.0)	96.35 (83.4)	99.7 (99.0)
Redundancy	4.5 (4.4)	11.1 (2.3)	8.7 (3.3)
Refinement			
Resolution (Å)	91.3-2.85	20.2-3.13	20.0-3.40
R_{work}/R_{free} (%)	25.3/30.1	24.5/33.7	28.2/37.2
No. reflections working/test set	24,550/1,241	18,481/942	15,050/760
No. atoms			
Protein	6,090	6,090	6,235
Ligands/ions	0/0	27/1	48/1
Water	379	259	444
Root mean square deviation			
Bond lengths (Å)	0.002	0.010	0.011
Bond angles (°)	0.57	1.36	1.45
Ramachandran plot (% favored/allowed/outliers)	89.7/8.2/2.1	87.2/11.1/1.7	80.8/16.8/2.4

[a] Values in parentheses correspond to the highest resolution shell.

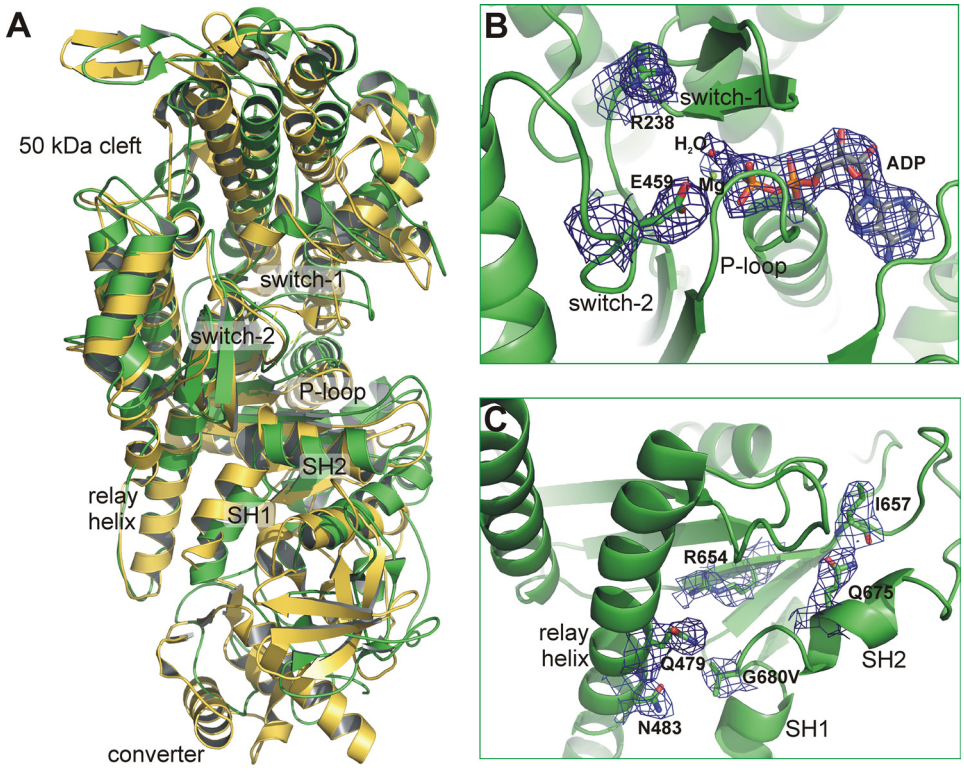

FIGURE 4. **Crystal structures of Gly-680 mutants.** *A*, shown is an overview of the G680A apo motor domain structure (*green*) superimposed on the wild-type myosin-2 x-ray structure in the apo state (*yellow*, PDB ID 2AKA). State-defining structural features are labeled. Note the differences in the state of the 50-kDa cleft, switch-1, and the reactive thiol region. *B*, shown is the structure of the ADP bound to the active site of G680A in the x-ray complex structure. Note the missing electron density for the γ-phosphate position despite the use of ADP and VO_3 during crystallization. Maps have been calculated with the nucleotide omitted. The salt bridge between Arg-238 and Glu-459, which is formed upon closure of the nucleotide binding pocket, is broken. *C*, the structure of the reactive thiol region in G680V is shown. Electron densities shown are the final $2F_o - F_c$ maps contoured at 1 σ.

and Switch-2 were found in positions to show the nucleotide binding pocket in the open state. The large 50-kDa cleft is open, and the relay helix is unkinked. Therefore, the converter and lever arm stay in the down position. Analysis of the normalized crystallographic B-factors showed a reduction in thermal mobility of certain parts of the myosin motor domain in the mutant structures, including most of the L50 kDa domain and especially the relay helix and Switch-2 (Fig. 6, *A*–*C*). The cooling effect is much more pronounced in the G680V mutant, which is consistent with a higher disturbance of myosin function in that mutant over G680A.

Molecular Dynamics Simulations and Principal Component Analysis—MD simulations were performed for the G680A, G680V, and wild-type myosin motor domains in explicit water using the Gromacs software suite (24) and the OPLS all-atom force field (25) to study the dynamic properties of the mutants

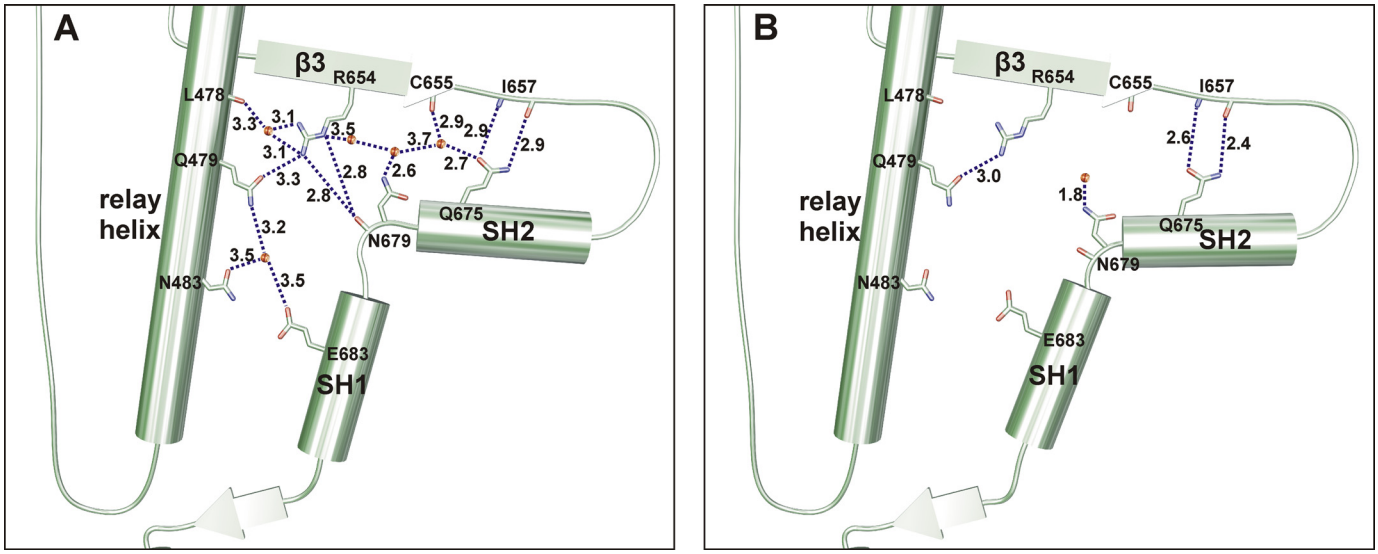

FIGURE 5. **Schematic representation of the interactions coupling the reactive thiol region to the surrounding structural elements.** *A*, shown is a wild-type interaction plot. *B*, shown are interactions in the Gly-680 mutants.

at room temperature. Analysis of the 100-ns trajectories shows the U50- and L50-kDa domains move toward each other to close the major cleft in the myosin motor domain of the Gly-680 mutants (Fig. 7). The closure of the cleft is mainly accomplished by a rotational movement of the U50-kDa domain of about 6–8 Å. Associated with the cleft closure, a rearrangement of Switch-1 in the active site of ~7 Å toward Switch-2 is observed. In contrast, the conformation of Switch-2 is stable over the simulation time and displays only minor fluctuations around its open position.

Principal component analysis of the trajectories was performed to identify large scale collective atomic fluctuations in the myosin motor domains. Principal component analysis is based on the computation of the covariance matrix of collective motions of atoms, and diagonalization of the covariance matrix leads to a matrix of eigenvectors and a set of eigenvalues. Projection of the motions corresponding to the eigenvectors on the G680A mutant structure is shown in Fig. 6*D*. The atomic fluctuations around the reactive thiol region, including the relay helix and Switch-2, are strikingly low. The diagonal of the covariance matrix represents the root mean square fluctuations of the system. A comparison of the root mean square fluctuations of the mutant motor domain *versus* wild type is given in Fig. 6*E*. The results are consistent with the crystallographic B-factor analysis and indicate that the Gly-680 mutation reduces the internal flexibility of the myosin motor domain.

In silico mutation of the wild-type *D. discoideum* myosin-2 motor domain to G680A and G680V, respectively, were carried out to analyze the influence of the mutation on the reactive thiol region. The mutated system was energy-minimized, and the explicit water molecules as well as the entire system was equilibrated before 100-ns MD simulations at 300 K. Along the trajectory, the SH1-helix together with the linker-loop started to move away from the relay helix and reached a final position about 2–3 Å away from its original position after ~50-ns simulation time. The SH2-helix was less affected at the C terminus, but the shift of the N-terminal end was more pronounced. The displacement of the reactive thiol region was higher in the case of replacing Gly-680 by valine.

DISCUSSION

Mutation of Gly-680 in *D. discoideum* myosin-2 and of the corresponding residue in other myosin isoforms notably affects the myosin activity and function. Nucleotide binding, hydrolysis, and product release are altered due to the mutation (11–15). Crystallographic analysis of the high resolution mutant x-ray structures reveals the G680A and G680V mutations to induce a conformation of the myosin motor domain, which resembles the wild-type ADP-bound state in the absence of actin. In contrast to wild-type myosin-2, the mutant myosins in their apo form show the large 50-kDa cleft in the motor domain in the open state. The relay helix is straight to facilitate the converter and lever arm to be in the down position. The active site is open, Switch-1 and Switch-2 moved away from each other, and the critical salt-bridge between Arg-238 and Glu-459 is broken.

The reactive thiol region serves as a hot spot for energetic coupling within the myosin motor domain. Gly-680 is located in the linker loop, which connects the SH1 and SH2 helices. Around the linker loop, an extensive network of interactions occurs in the wild-type myosin between the reactive thiol region, the relay helix, and the central β-sheet. This network involves at least nine protein residues and five water molecules. The introduction of an aliphatic side chain, like the methyl group in alanine or the isopropyl group in valine, seems to sterically push the reactive thiol region away from the relay helix and the transducer. Because of this displacement, most of the hydrogen bonds can no longer be formed, and the gap between relay helix and the reactive thiol region widens.

The results of *in silico* mutation and the subsequent 100-ns MD simulations at 300 K support the mechanism of a mutational-induced displacement of the reactive thiol region away from the relay helix and the transducer. Thereby, the reactive thiol region loses its function in energetic transmission and in mediating conformational changes within the myosin motor

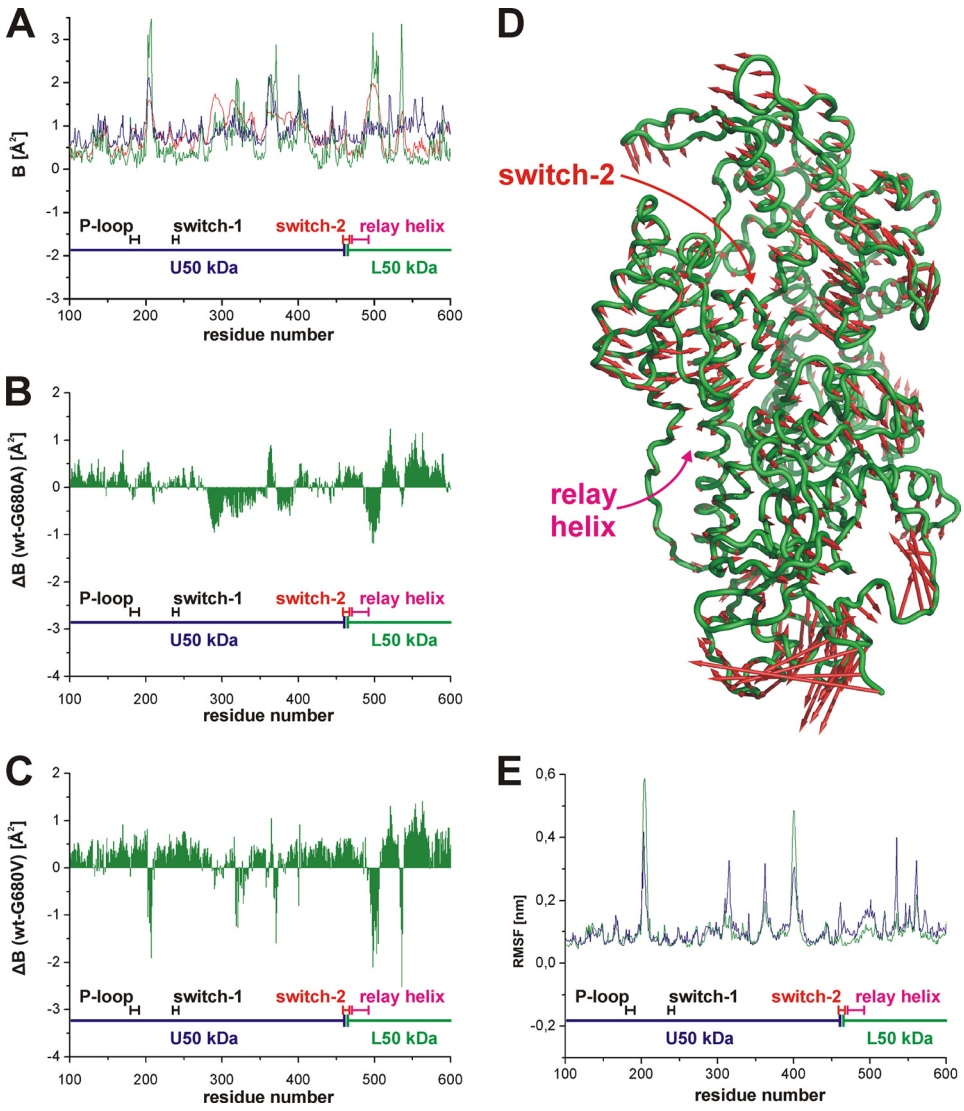

FIGURE 6. **Analysis of fluctuations and internal mobility in the mutant and wild-type myosins.** *A*, shown is a diagram of the normalized crystallographic B-factors against the residue number of wild type (*blue*), G680A (*red*), and G680V (*green*). Normalization has been performed by dividing the residual B-factors by the average of the B-factors in the chain as $B_{norm} = (B_{x\text{-}ray}/\langle B_{x\text{-}ray}\rangle)$. Note the decrease in B-factors in the L50-kDa domain, the relay helix, and Switch-2. *B*, shown is a histogram of Δ*B* (wild type-G680A). *C*, shown is a histogram of ΔB (wild type-G680V). The effect is notably higher in the G680V mutant. *D*, shown is a representation of the first eigenvector obtained by principal component analysis of the MD trajectories plotted as displacement vectors attached to the C_α atoms of G680A. The protein is shown in tube representation. Both the relay helix and Switch-2 show minor mobility. *E*, shown is a root mean square fluctuations (*RMSF*) diagram of wild-type (*blue*) and G680A (*green*) calculated from MD trajectories.

domain, which are crucial for lever arm movement and force generation.

Moreover, refinement of the crystal structure of G680A crystallized in the presence of 2 mM ADP and 2 mM sodium VO_3 exhibited no electron density for the γ-phosphate mimicking *meta*-vanadate in the nucleotide binding pocket but only for ADP. This is very unusual, as the *meta*-vanadate is clearly visible in known wild-type myosin-2 structures that were obtained in the presence of ADP-VO_3, like *e.g.* PDB IDs 2JJ9, 2JHR, and 2XO8. Generally, the addition of ADP-VO_3 traps the wild-type myosin motor domain in a well defined state and, hence, facilitates crystallization.

Transient kinetics show an increased affinity of the G680A mutant over wild-type constructs in the absence of actin and a 100-fold decreased ADP dissociation rate. ADP is tightly bound to the active site, in fact, tighter than to the wild type, $\Delta\Delta G^\circ =$ 3.3 kJ·mol^{-1}, with an increased enthalpic contribution ΔH° of about 18–19 kJ·mol^{-1} (~25%). In the presence of actin the affinity of the wild-type myosin for ADP decreases dramatically (from 7 to ~240 μM), whereas the affinity of the mutant constructs remains largely unchanged or even increases slightly. Calculation of the thermodynamic parameters shows that the energy barrier $\Delta H^\ddagger$ for ADP binding is reduced by actin, but the free energy of ADP binding ΔG° is unchanged. Despite similar affinities for G680A in the presence or absence of actin, the entropies are very different, and in the presence of actin the binding of ADP is enthalpy-driven. The entropy $T\Delta S^\circ$ of ADP binding is considerably reduced in the G680A construct. On the one hand, the reduction in entropy is caused to a high degree by the tighter binding of the nucleotide to the myosin pocket and the accompanied loss of mobility. On the other hand, the entropic term is not solely composed of the substrate

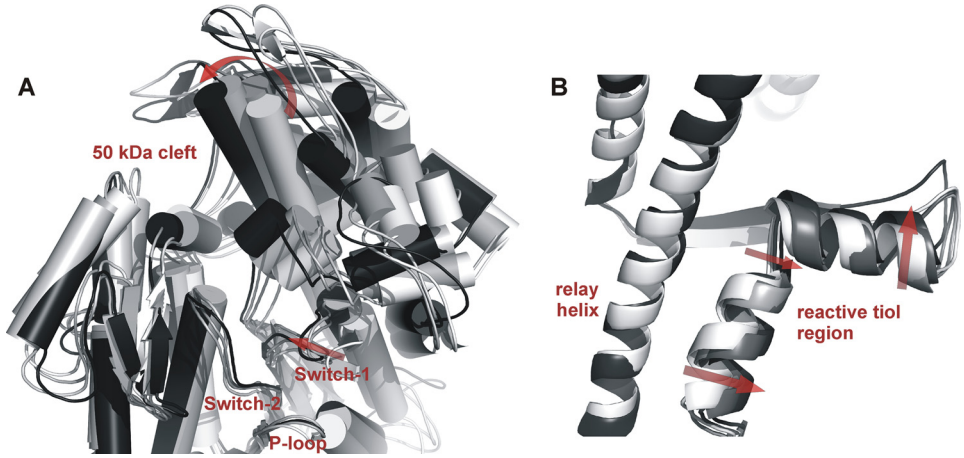

FIGURE 7. **Snapshots from the MD simulations at 300 K.** *A*, the U50-kDa domain of G680A rotates to close the major cleft in the motor domain along the trajectory. Switch-1 changes its conformation, whereas the position of Switch-2 is stable. *Red arrows* indicate the movements of the U50-kDa domain and Switch-1. *B*, the reactive thiol region clearly moves away from the relay helix during 100 ns of *in silico*-mutated myosin MD simulations. The starting and end positions of the MD simulations are shown in *white* and *black*. Intermediate structures along the trajectory are given in *gray*. *Red arrows* indicate the displacement of the reactive thiol region.

contribution, but also the expulsion of water molecules from the active site or changes in the flexibility of surrounding amino acids are of notable importance.

To study the dynamic behavior of the active site and the motor domain in general, we used MD simulations of the G680A and G680V mutants in aqueous solution based on the two apo form x-ray structures. Over the 100-ns simulation time, the position of Switch-2 is stable, whereas Switch-1 changes its conformation and moves toward Switch-2. The rearrangement of Switch-1 is associated with a rotation of the entire U50-kDa domain and the process of closing the 50-kDa cleft. This behavior has been observed in all MD simulations performed with the mutant myosin motor domains.

The crystallographic B-factors as well as principal component analysis of the MD trajectories indicate a reduction in thermal flexibility or mobility of parts of the L50-kDa domain including the relay helix and Switch-2. Therefore, we hypothesize that the Gly-680 mutants are still capable of closing the 50-kDa cleft upon interaction with actin and thereby changing the conformation of Switch-1. This assumption is supported by the fact that actin still holds the ability to accelerate ADP binding and release in stopped flow measurements (11). The open cleft and the observed position of Switch-1 in the mutant x-ray structures seem to be defined by the crystallization conditions. However, Switch-2 and the adjacent relay helix appear to be trapped or frozen in one particular position due to the mutation. Hence, the impairment of the γ-phosphate-sensing function of Switch-2 leads to a reduction of the rate constants of nucleotide binding to the mutant myosin. The associated decrease of thermal flexibility might be responsible for the possibility to rescue the slow movement of F-actin by myosin mutants in *in vitro* motility assays at elevated temperatures (12, 15) and might contribute to the reduced entropy of ADP binding.

In addition, a number of intragenic suppressor mutations have been reported that restore almost normal myosin function of the Gly-680 mutants (37, 38). The suppressor mutations compensate for the defects caused by the single-point mutation at position Gly-680 and can be roughly classified into two groups depending on their location in the myosin motor domain. One group of mutants (M91I, G120C, L123F, E476Q, N483S, and L676F) clusters in structural elements, like the relay helix, parts of the transducer or helices in the L50- and U50-kDa domains, around the reactive thiol region. These rescue mutations are positioned in such a way that they might support interactions of the reactive thiol region with its neighboring elements and recouple the reactive thiol region of the mutants to the motor. On first glance, the other group of suppressors (P128Q, L175F, L176F, I177M, G182C, T189I, V192F, I193M, L216F, N235D, G240N/C/V, L453F/Y, and L638F) appears to be randomly located in the motor domain. However, mapping these mutations on the Gly-680 mutant structures, they can be found in several strands of the central β-sheet and in strategically important positions to influence the active site and the chemomechanical coupling within the motor domain.

In conclusion, the Gly-680 mutations stabilize occupancy of an ADP-like state. ADP is tightly bound to the active site with increased enthalpic and reduced entropic contributions assisting in stronger binding. The Gly-680 mutations lead to uncoupling of the reactive thiol region from the surrounding elements and reduce the thermal mobility in parts of the myosin motor domain. In particular, the relay helix and Switch-2 are affected by the "freezing" or "trapping" that is responsible for many of the kinetic and functional defects observed for the mutant myosins. Our results explain how moderate increases in temperature can compensate for this freezing effect and suppress many of the mutant defects.

Acknowledgments—We thank the European Synchrotron Radiation Facility for provision of synchrotron radiation facilities, Christian Riekel for assistance in using beamline ID13, and Sean Mc Sweeney for assistance in using beamline ID23–2. We thank Joachim Greipel and Andreas Blaskowitz for help, Petra Baruch for technical assistance, and Krishna Chinthalapudi and Sarah M. Heissler for helpful discussions.

REFERENCES

1. Wells, J. A., Sheldon, M., and Yount, R. G. (1980) *J. Biol. Chem.* **255,** 1598–1602
2. Huston, E. E., Grammer, J. C., and Yount, R. G. (1988) *Biochemistry* **27,** 8945–8952
3. Liang, W., and Spudich, J. A. (1998) *Proc. Natl. Acad. Sci. U.S.A.* **95,** 12844–12847
4. Wells, J. A., and Yount, R. G. (1979) *Proc. Natl. Acad. Sci. U.S.A.* **76,** 4966–4970
5. Dalbey, R. E., Weiel, J., and Yount, R. G. (1983) *Biochemistry* **22,** 4696–4706
6. Titus, M. A., Ashiba, G., and Szent-Györgyi, A. G. (1989) *J. Muscle Res. Cell Motil.* **10,** 25–33
7. DeLozanne, A., Lewis, M., Spudich, J. A., and Leinwand, L. A. (1985) *Proc. Natl. Acad. Sci. U.S.A.* **82,** 6807–6810
8. Rayment, I., Holden, H. M., Whittaker, M., Yohn, C. B., Lorenz, M., Holmes, K. C., and Milligan, R. A. (1993) *Science* **261,** 58–65
9. Giese, K. C., and Spudich, J. A. (1997) *Biochemistry* **36,** 8465–8473
10. Uyeda, T. Q., Tokuraku, K., Kaseda, K., Webb, M. R., and Patterson, B. (2002) *Biochemistry* **41,** 9525–9534
11. Batra, R., Geeves, M. A., and Manstein, D. J. (1999) *Biochemistry* **38,** 6126–6134
12. Patterson, B., and Spudich, J. A. (1995) *Genetics* **140,** 505–515
13. Kinose, F., Wang, S. X., Kidambi, U. S., Moncman, C. L., and Winkelmann, D. A. (1996) *J. Cell Biol.* **134,** 895–909
14. Patterson, B., Ruppel, K. M., Wu, Y., and Spudich, J. A. (1997) *J. Biol. Chem.* **272,** 27612–27617
15. Patterson, B., and Spudich, J. A. (1996) *Genetics* **143,** 801–810
16. Manstein, D. J., and Hunt, D. M. (1995) *J. Muscle Res. Cell Motil.* **16,** 325–332
17. Lehrer, S. S., and Kerwar, G. (1972) *Biochemistry* **11,** 1211–1217
18. Criddle, A. H., Geeves, M. A., and Jeffries, T. (1985) *Biochem. J.* **232,** 343–349
19. Kabsch, W. (1993) *J. Appl. Crystallogr.* **26,** 795–800
20. Navaza, J. (1994) *Acta Crystallogr. Sect. A: Found. Crystallogr.* **50,** 157–163
21. Murshudov, G. N., Vagin, A. A., and Dodson, E. J. (1997) *Acta Crystallogr. D. Biol. Crystallogr.* **53,** 240–255
22. Adams, P. D., Afonine, P. V., Bunkóczi, G., Chen, V. B., Davis, I. W., Echols, N., Headd, J. J., Hung, L. W., Kapral, G. J., Grosse-Kunstleve, R. W., McCoy, A. J., Moriarty, N. W., Oeffner, R., Read, R. J., Richardson, D. C., Richardson, J. S., Terwilliger, T. C., and Zwart, P. H. (2010) *Acta Crystallogr. D. Biol. Crystallogr.* **66,** 213–221
23. Emsley, P., Lohkamp, B., Scott, W. G., and Cowtan, K. (2010) *Acta Crystallogr. D. Biol. Crystallogr.* **66,** 486–501
24. Hess, B., Kutzner, C., van der Spoel, D., and Lindahl, E. (2008) *J. Chem. Theory Comput.* **4,** 435–447
25. Jorgensen, W. L., Maxwell, D. S., and Tirado-Rives, J. (1996) *J. Am. Chem. Soc.* **118,** 11225–11236
26. Jorgensen, W. L., Chandrasekhar, J., Madura, J. D., Impey, R. W., and Klein, M. L. (1983) *J. Chem. Phys.* **79,** 926–935
27. Darden, T., York, D., and Pedersen, L. (1993) *J. Chem. Phys.* **98,** 10089–10092
28. Hess, B., Bekker, H., Berendsen, H. J. C., and Fraaije, J. G. E. M. (1997) *J. Comp. Chem.* **18,** 1463–1472
29. Reubold, T. F., Eschenburg, S., Becker, A., Kull, F. J., and Manstein, D. J. (2003) *Nat. Struct. Biol.* **10,** 826–830
30. Yang, Y., Gourinath, S., Kovács, M., Nyitray, L., Reutzel, R., Himmel, D. M., O'Neall-Hennessey, E., Reshetnikova, L., Szent-Györgyi, A. G., Brown, J. H., and Cohen, C. (2007) *Structure* **15,** 553–564
31. Coureux, P. D., Wells, A. L., Ménétrey, J., Yengo, C. M., Morris, C. A., Sweeney, H. L., and Houdusse, A. (2003) *Nature* **425,** 419–423
32. Coureux, P. D., Sweeney, H. L., and Houdusse, A. (2004) *EMBO J.* **23,** 4527–4537
33. Gulick, A. M., Bauer, C. B., Thoden, J. B., and Rayment, I. (1997) *Biochemistry* **36,** 11619–11628
34. Niemann, H. H., Knetsch, M. L., Scherer, A., Manstein, D. J., and Kull, F. J. (2001) *EMBO J.* **20,** 5813–5821
35. Bauer, C. B., Holden, H. M., Thoden, J. B., Smith, R., and Rayment, I. (2000) *J. Biol. Chem.* **275,** 38494–38499
36. Bauer, C. B., Kuhlman, P. A., Bagshaw, C. R., and Rayment, I. (1997) *J. Mol. Biol.* **274,** 394–407
37. Patterson, B. (1998) *Genetics* **149,** 1799–1807
38. Wu, Y., Nejad, M., and Patterson, B. (1999) *Genetics* **153,** 107–116